Inelastic neutron scattering study of crystal field excitations of Nd^{3+} in NdFeAsO

Y. Xiao,[1,*] M. Zbiri,[2,†] R. A. Downie,[3] J.-W. G. Bos,[3] Th. Brückel,[1] and T. Chatterji[2,‡]

[1]*Jülich Centre for Neutron Science JCNS and Peter Grünberg Institut PGI, JARA-FIT, Forschungszentrum Jülich GmbH, D-52425 Jülich, Germany*

[2]*Institut Max von Laue–Paul Langevin, 6 rue Jules Horowitz, BP 156, 38042 Grenoble Cedex 9, France*

[3]*Institute of Chemical Sciences and Centre for Advanced Energy Storage and Recovery, School of Engineering and Physical Sciences, Heriot-Watt University, Edinburgh EH14 4AS, United Kingdom*

(Received 27 September 2013; revised manuscript received 22 November 2013; published 19 December 2013)

Inelastic neutron scattering experiments were performed to investigate the crystalline electric field (CEF) excitations of Nd^{3+} ($J = 9/2$) in the iron pnictide NdFeAsO. The crystal field level structures for both the high-temperature paramagnetic phase and the low-temperature antiferromagnetic phase of NdFeAsO are constructed. The variation of CEF excitations of Nd^{3+} reflects not only the change of local symmetry but also the change of magnetic ordered state of the Fe sublattice. By analyzing the crystal field interaction with a crystal field Hamiltonian, the crystal field parameters are obtained. It was found that the sign of the fourth- and sixth-order crystal field parameters change upon the magnetic phase transition at ∼140 K, which may be due to the variation of exchange interactions between the 4*f* and conduction electrons.

DOI: 10.1103/PhysRevB.88.214419 PACS number(s): 78.70.Nx, 71.70.Ch, 74.70.Xa

I. INTRODUCTION

The discovery of superconductivity at $T_c = 26$ K in $LaFeAsO_{1-x}F_x$ has triggered extensive research on the physical properties and the superconducting mechanism of Fe-based superconductors.[1,2] Superconducting transition temperatures higher than 50 K can be reached if the nonmagnetic La atom is replaced by a magnetic rare-earth element *R*, such as Pr, Nd, and Sm.[3–6] The resulting enhancement of T_c is mostly due to the variation of the geometric factors rather than the rare-earth magnetism.[2,7,8] Nevertheless, the interplay between the Fe 3*d* and rare-earth 4*f* magnetism in Fe pnictides still plays an important role in determining the structural and physical properties of these materials. For instance, strong couplings between rare-earth and Fe magnetism are observed in both CeFeAsO and SmFeAsO parent compounds.[8,9] For the specific case of NdFeAsO, the Fe spin-density-wave (SDW) transition at $T_{SDW} = 137$ K is found to be preceded by a tetragonal-to-orthorhombic structural phase transition at $T_S = 142$ K. A spin-reorientation of the Fe magnetic sublattice takes place upon the ordering of the Nd moments at low temperature.[10–13]

As a major interaction in rare-earth compounds, the crystalline electric field (CEF) interaction reflects directly the electrical and magnetic potential on the rare-earth site, which is created by neighboring ions.[14,15] The experimental determination of the structure and parameters of CEF is of a considerable importance in order to get deeper insights into the related energy scale, and therefore to enhance the understanding of the physical properties of rare-earth contained compounds, based on the degeneracy of the CEF states. As the CEF interaction in the NdFeAsO parent phase has to date not been investigated, we have probed the crystal field excitations of Nd^{3+} in NdFeAsO by means of inelastic neutron scattering. By performing a CEF analysis with a single-ion model Hamiltonian, the crystal field levels are established and the related parameters are extracted for both the paramagnetic and antiferromagnetic phases. The ground state of the Nd^{3+} ion was found to be a magnetic doublet in the high-temperature paramagnetic phase, while the molecular field generated by the long-range order of the Fe moments lifts the degeneracy further, resulting in a magnetic singlet ground state in the low-temperature antiferromagnetic phase. It was also found that both fourth- and sixth-rank crystal field interactions are quite different due to the variation of rare-earth conduction electron interactions in the two different phases.

II. EXPERIMENTAL DETAILS

Polycrystalline sample of NdFeAsO was prepared by standard solid state chemistry methods as previously reported.[16] The powder NdFeAsO sample was examined by laboratory x-ray diffraction (XRD) on a Huber G670 Guinier imaging plate diffractometer with Cu $K\alpha$ radiation and a Ge(111) monochromator. The inelastic neutron scattering measurements were performed, in the temperature range from 1.6 to 200 K, on the direct-geometry thermal-neutron time-of-flight spectrometer IN4C at the Institut Laue Langevin (Grenoble, France). In order to cover an extended *Q* range and to gain in energy resolution, two incident wavelengths of $\lambda_i = 1.11$ and 2.22 Å were selected using a pyrolitic graphite monochromator. About 7 g of NdFeAsO powder sample was put inside a thin aluminum sample holder that was fixed to the cold tip of the sample stick of a standard orange cryostat. Standard corrections including detector efficiency calibration and background substraction were performed. The data analysis was done using ILL software tools. The temperature dependence of the magnetic susceptibility of the NdFeAsO sample was measured on a Quantum Design magnetic property measurement system (MPMS-XL5) in the temperature range from 2 to 300 K.

III. RESULTS AND DISCUSSION

The x-ray diffraction pattern of the NdFeAsO powder sample at room temperature is shown in Fig. 1. The compound crystalizes in the tetragonal ZrCuSiAs-type structure with space group $P4/nmm$. Rietveld refinement of the crystal

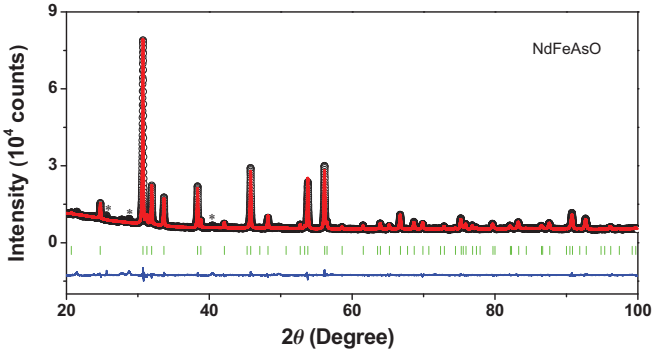

FIG. 1. (Color online) The room-temperature XRD refinement pattern for NdFeAsO. The vertical bars at the bottom indicate the Bragg reflection positions. The lowest curve is the difference between the observed and the calculated patterns. The reflections originating from impurities are marked with asterisks.

structure leads to lattice parameters of $a = 3.965(2)$ and $c = 8.587(2)$ Å. The lattice parameters derived from XRD measurements are in good agreement with our previous work.[16] Further, the XRD pattern exhibits few weak peaks arising from Nd_2O_3 and FeAs impurities. Since the amount of the impurity phase is small with a total weight fraction of less than 5%, it will not affect the inelastic neutron spectra and the CEF analysis of the main phase of NdFeAsO.

Figures 2(a) and 2(b) show the Bose-factor-corrected $S(Q,\omega)$ plots for NdFeAsO at 5 and 160 K, respectively. Above T_{SDW}, both the lattice and CEF excitations contribute to the spectra. Below T_{SDW}, the neutron scattering intensity contains also a contribution of magnon scattering. Other inelastic neutron scattering studies of Fe pnictides have shown that the integrated cross sections of the Fe spin wave excitations in these materials are relatively small compared to that of phonon and CEF excitations.[17,18] Therefore, the CEF and lattice (phonon) excitations dominate the neutron spectra while the magnon scattering can be neglected during the data analysis, as presently done. The generalized phonon density of states (GDOS)[19] was collected using an incident neutron wavelength $\lambda_i = 1.11$ Å. The GDOS [Fig. 2(c)] was extracted from the angle-integrated data over the high-Q region of the (Q,ω) space. The incoherent approximation is applied in the same way as in previous works dealing with phonon dynamics in Fe pnictides.[20–23] Our phonon spectra agree well with other measurements on NdFeAsO and $NdFeAsO_{1-x}F_x$ using inelastic x-ray scattering techniques.[24] Further, the present GDOS shows similar features as those of the isostructural $LaFeAsO_{1-x}F_x$ compound obtained via inelastic neutron scattering measurements.[25] One can notice that, upon the structural phase transition, the observed phonon features change only slightly. It is known that the phonon scattering intensity generally increases proportional to Q^2. Pure CEF excitations, which are not coupled to propagating modes, are local excitations. They do not possess a characteristic dispersion, and the scattering intensity decreases with Q following a magnetic form factor. By considering the different Q-dependence behaviors of phonon and CEF excitations, the contribution from CEF excitations can be separated by subtracting the high-Q spectra which contain

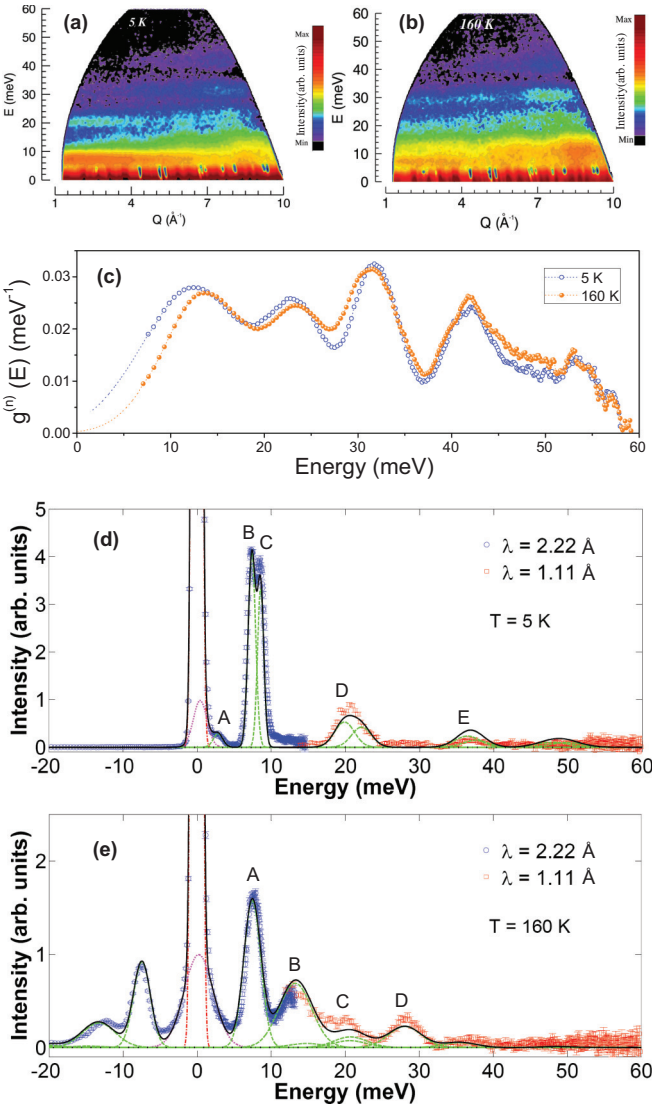

FIG. 2. (Color online) (a) and (b) The experimental Bose-factor corrected $S(Q,\omega)$ plots for NdFeAsO at 5 and 160 K obtained using an incident neutron wavelength of 1.11 Å. For clarity, a logarithmic representation is used for the intensities. (c) The experimentally generalized phonon density of states (GDOS) at 5 and 160 K for NdFeAsO. The GDOS was extracted within the incoherent approximation framework where the data was angle-averaged over the high-Q region of the (Q,ω) space of (a) and (b), i.e., $7 \leqslant Q \leqslant 10$ Å^{-1}. (d) and (e) Energy spectra of the CEF excitations of NdFeAsO at 5 and 160 K. The dash-dotted lines denote the elastic scattering line, the dotted line denotes the quasielastic scattering line shape fit, the dashed lines represent the fit of individual CEF transitions as described in the text, and the solid line is a fit of the whole inelastic neutron scattering spectrum. The labeled peaks correspond to the representative CEF transitions marked in Fig. 3(b).

phonon scattering from the low-Q spectra corresponding to both CEF and phonon scattering, as described in Ref. 26. Thus, the CEF scattering in NdFeAsO are presently obtained by subtracting the data summed over the high-Q range of $7 \leqslant Q \leqslant 8.4$ Å^{-1} from the low-angle data summed over the low-Q range of $2.8 \leqslant Q \leqslant 4.2$ Å^{-1}, after scaling by a constant factor at each temperature.

The obtained CEF excitation spectra at 5 and 160 K are shown in Figs. 2(d) and 2(e) as plots of the energy dependence of the scattering intensity. With increasing temperature, the intensities of all inelastic peaks in Fig. 2(d) are decreased, indicating that these peaks originate from the excitations between the ground state to excited states. As the temperature increases to 160 K, few new peaks are observed and their intensity increases with increasing temperature. These peaks can be assigned to the CEF transitions between the populated excited states. Further, the deexcitation transition from the excited states to the ground state can be also observed on the neutron energy gain side (negative energy) of the spectra in Fig. 2(e). The dynamic structure factors of the neutron energy gain and neutron energy loss processes are related to each other through the principle of detailed balance, i.e., $S(-\omega) = e^{-\hbar\omega/kT} S(\omega)$. To interpret the CEF spectra, we analyze the data in the framework of the following ionic CEF model Hamiltonian:

$$\hat{H} = \hat{H}_{\mathrm{CEF}} + 2\mu_B(g_J - 1)B_{\mathrm{mol}}\hat{J}, \qquad (1)$$

where $\hat{H}_{\mathrm{CEF}}$ represents the crystalline electric field Hamiltonian, which describes the CEF interaction at the Nd^{3+} site in the NdFeAsO compound. The second term is the contribution of a molecular magnetic field coupling to the total angular momentum $\hat{J}$ of the Nd^{3+} ion.

In the high-temperature tetragonal phase, the Nd^{3+} cations are located at the $2c$ site under the C_{4v} local symmetry. The corresponding CEF Hamiltonian can be written as $\hat{H}_{\mathrm{CEF}}^{\mathrm{Tetr.}} = B_2^0\hat{O}_2^0 + B_4^0\hat{O}_4^0 + B_4^4\hat{O}_4^4 + B_6^0\hat{O}_6^0 + B_6^4\hat{O}_6^4$, where the B_n^m are the CEF parameters and the $\hat{O}_n^m$ are the CEF Stevens equivalent operators as defined in Ref. 27. The crystal field of the C_{4v} symmetry splits the tenfold multiplets of a free Nd^{3+} ion into three Γ_6 and two Γ_7 Kramers doublets. In the low-temperature orthorhombic phase, the Nd^{3+} $^4I_{9/2}$ ground multiplets are split by the orthorhombic crystal field of the C_{2v} symmetry into five Kramers doublets, namely five Γ_5 states. The CEF Hamiltonian reads as $\hat{H}_{\mathrm{CEF}}^{\mathrm{Orth.}} = B_2^0\hat{O}_2^0 + B_2^2\hat{O}_2^2 + B_4^0\hat{O}_4^0 + B_4^2\hat{O}_4^2 + B_4^4\hat{O}_4^4 + B_6^0\hat{O}_6^0 + B_6^2\hat{O}_6^2 + B_6^4\hat{O}_6^4 + B_6^6\hat{O}_6^6$. In principle, four CEF excitation peaks are expected to be observed at 5 K. Any further splitting of CEF peaks in the orthorhombic phase would indicate that the molecular field, i.e., the effective exchange magnetic field B_{mol} induced by the Fe magnetic sublattice, plays an important role, and the degeneracy would be further lifted. The local structure surrounding the Nd^{3+} ion at 5 K is illustrated in Fig. 3(a).

Within the dipole approximation, the differential cross-section for unpolarized neutron scattering and for a CEF transition from state $|i\rangle$ to $|j\rangle$ can be expressed as

$$\frac{d^2\sigma(i \to j)}{d\Omega dE'} = N\frac{k_f}{k_i}\left(\frac{\hbar\gamma e^2}{mc^2}\right)^2 e^{-2W}\left|\frac{1}{2}g_J F(\mathbf{Q})\right|^2 \times \sum_{i,j} n_i |\langle j|J_\perp|i\rangle|^2 \delta(E_i - E_j + \hbar\omega), \qquad (2)$$

where k_i and k_f are the initial and final neutron wave vectors, and $\hbar\omega$ is the energy transfer. γ is the neutron gyromagnetic ratio, e^2/mc^2 is the classical electron radius, g_J is the Landé factor, $F(\mathbf{Q})$ is the magnetic form factor, e^{-2W} is the Debye-Waller factor, n_i is the probability distribution of initial states, and $J_\perp$ is the component of the total angular-momentum operator perpendicular to $\mathbf{Q}$. The powder-averaged cross section Eq. (2) can be used for a direct comparison with the CEF scattering data obtained using a polycrystalline sample. By taking into account the observed CEF energy positions, transition intensities, and the evolution of the spectra as a function of temperature, a relevant fit is performed allowing us to obtain reliable crystal field parameters that can be used to describe the behavior of the CEF excitations in NdFeAsO.[28] As indicated by the solid lines in Figs. 2(d) and 2(e), the results of the fitting lead to a good agreement with the observed spectra. Two sets of CEF parameters are obtained, at 5 and 160 K, and listed in Table I. A schematic diagram of the splitting of the Nd^{3+} $^4I_{9/2}$ ground multiplet is presented in Fig. 3(b). Clearly, the ground state at 5 K is a magnetic singlet, whereas the ground state at 160 K is a magnetic doublet. Usually, the different ground states would result in a different quasielastic scattering behavior. The comparison of the neutron spectra at 5 K [Fig. 2(d)] and at 160 K [Fig. 2(e)] highlights the noticeable appearance of a considerable quasielastic peak intensity nearby the resolution limit of the elastic peak. The quasielastic signal can be understood as being due to the spin fluctuations occurring within the degenerate ground state of Nd^{3+} ions. It favors the multiplet ground state. The strong quasielastic peak observed at 160 K is mainly due to

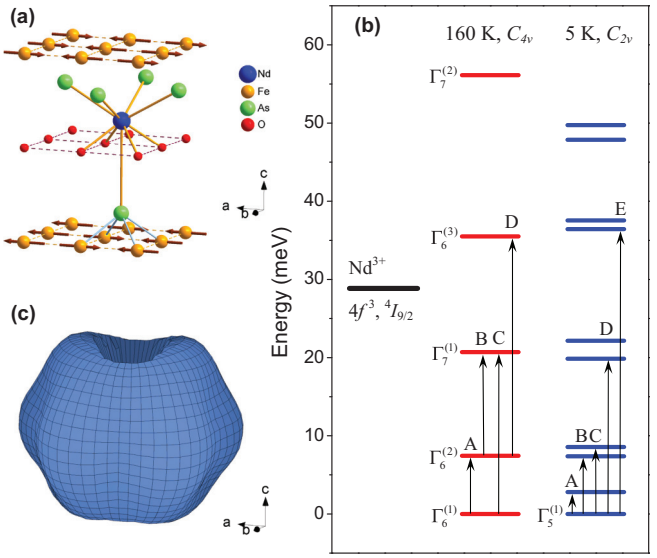

FIG. 3. (Color online) (a) Illustration of the local structure of the Nd^{3+} ion at 5 K. It is subject to a crystal electric field generated by the neighboring arsenic and oxygen ions, and a molecular field induced by the long-range order of the iron spins. (b) Scheme of the energy-levels of Nd^{3+} cations in NdFeAsO for the lowest J multiplets under the tetragonal and orthorhombic structural environments, as derived from neutron spectroscopy. The values of energies at 160 K are sorted in increasing order: 0, 7.45, 20.69, 35.51, and 56.12 meV. Similarly, we show the energies at 5 K: 0, 2.81, 7.38, 8.56, 19.86, 22.16, 36.44, 37.55, 47.86, and 49.75 meV. It is noted that the excitations between any Γ_6 and Γ_7 states are allowed by the selection rules of neutron scattering at 160 K. The arrows indicate few representative CEF transitions as extracted from our neutron spectra. (c) The charge density distribution of Nd^{3+} in NdFeAsO at 5 K.

TABLE I. The CEF parameters (meV) of NdFeAsO at 5 and 160 K. The molecular fields obtained at 5 K are $B^x_{\rm mol} = 11.2(3)$ T, $B^z_{\rm mol} = 11.7(3)$ T.

	B^0_2	B^2_2	B^0_4	B^2_4	B^4_4	B^0_6	B^2_6	B^4_6	B^6_6
5 K	−0.567(9)	$4.1(3)\times10^{-2}$	$1.1(2)\times10^{-3}$	$-8.8(3)\times10^{-3}$	$-3.2(2)\times10^{-2}$	$-8.6(5)\times10^{-5}$	$5.1(4)\times10^{-4}$	$6.7(4)\times10^{-4}$	$1.9(3)\times10^{-3}$
160 K	−0.584(9)		$-2.6(3)\times10^{-3}$		$-5.7(3)\times10^{-2}$	$1.5(5)\times10^{-4}$		$4.6(5)\times10^{-4}$	

the magnetic doublet ground state with wave function $\psi_g = 0.2505|\frac{9}{2}, \pm\frac{1}{2}\rangle + 0.2239|\frac{9}{2}, \mp\frac{7}{2}\rangle + 0.9419|\frac{9}{2}, \pm\frac{9}{2}\rangle$, whereas the ground state at 5 K is a magnetic singlet with wave function $\psi_g = 0.9585|\frac{9}{2}, -\frac{9}{2}\rangle - 0.0403|\frac{9}{2}, -\frac{7}{2}\rangle - 0.1268|\frac{9}{2}, -\frac{5}{2}\rangle + 0.0144|\frac{9}{2}, -\frac{3}{2}\rangle + 0.0255|\frac{9}{2}, -\frac{1}{2}\rangle - 0.0028|\frac{9}{2}, \frac{1}{2}\rangle - 0.2467|\frac{9}{2}, \frac{3}{2}\rangle + 0.0344|\frac{9}{2}, \frac{5}{2}\rangle + 0.0198|\frac{9}{2}, \frac{7}{2}\rangle - 0.0173|\frac{9}{2}, \frac{9}{2}\rangle$.

Generally, the CEF parameters of insulating materials can be obtained from point-charge-model based calculations.[29] It is assumed that the wave functions of the 4*f* and the neighboring ions do not overlap, and the electrostatic crystal field potential is only created by the charge distribution of the neighboring ions. However, in metallic systems, the conduction electrons screen out the neighboring ionic point charge contribution, and the interaction between the 4*f* and the conduction electrons plays an important role in the determination of CEF parameters. At the rare-earth sites, the conduction and the 4*f* electrons interact via direct and exchange Coulomb interactions.[30–32] It was found that the exchange coulombic contribution of the conduction electrons to the CEF in rare-earth intermetallics may counterbalance the direct Coulomb contribution. Therefore, this would change the sign and magnitude of the effective CEF parameters B^0_4 and B^0_6.[32,33] By comparing the CEF parameters obtained at 5 and 160 K, the B^0_2, B^4_4, and B^4_6 are found to not exhibit a strong variation at the two different phases, while both the sign and magnitude of B^0_4 and B^0_6 are affected. It is suggested that the exchange contribution is larger in the antiferromagnetic phase than in the paramagnetic phase of the metallic NdFeAsO system due to the stronger overlap of the radial wave functions of the 4*f* and conduction electrons.

The CEF parameters determined from our inelastic neutron scattering measurements, at 5 K, allowed us to calculate the spatial charge density distribution of the 4*f* electrons of Nd^{3+} in NdFeAsO.[34] As illustrated in Fig. 3(c), the charge density distribution is significantly nonspherical with a slight variation in the *ab* plane, and a large contraction along the *c* axis. The distortion of the charge density by CEF will lead to the magnetocrystalline anisotropy of the compound. Given the fact that the Nd^{3+} cations possess a negative second-order Stevens factor α_J, the easy-axis anisotropy of the Nd magnetic sublattice at 5 K is expected to be along the *c* axis. This is similar to the case of the isostructural SmFeAsO and CeFeAsO compounds, where the moment directions of the Sm and Ce atoms were determined to be along the *c* axis, between T_N^{RE} and $T_{\rm SDW}$.[8,9] The rare-earth magnetic order in this temperature range was confirmed to be induced by the 3*d*-4*f* exchange interactions.

Extensive research efforts have been made to understand the role the rare-earth elements played in the emergence of the physical properties of the rare-earth-containing iron oxyarsenides, as well as the effects and significance of the correlation between the rare-earth and iron magnetism. From the analysis of the low-energy spin excitations in the undoped CeFeAsO, using a Heisenberg model,[35] it is argued that the magnetic coupling between the Ce and Fe spins is negligible. However, the investigation of the CEF excitations in CeFeAsO confirmed the occurrence of an interplay between Ce and Fe magnetic ions since the molecular field of the Fe spins acting on the Ce ions is deduced to be larger than 1 meV.[17] The discrepancy may be due to the underestimation of Ce-Fe exchange interaction,[35] as the Ce spin wave excitation might not be sensitive to the Ce-Fe coupling. Regarding to NdFeAsO compound, the interplay between Nd and Fe magnetism is complex and is more pronounced as the order-order transition of the Fe magnetic sublattice exhibits a closer proximity to the onset of the Nd magnetic order.[11] In the present work, the Fe molecular field acting on the Nd ions is found to be around 11 T at 5 K. The magnitude of the molecular field in NdFeAsO is similar to that in CeFeAsO,[17] highlighting the importance of the coupling between the rare-earth and iron ions, as well as the very similar Fe magnetism in the rare-earth-containing iron oxyarsenides.

In order to get deeper insights into the effect of the molecular field of the Fe atoms on the CEF excitations, a plot of $S(Q,\omega)$ at 5 K, obtained from better energy resolution data (incident neutron wavelength of 2.22 Å) is shown in Fig. 4(a).

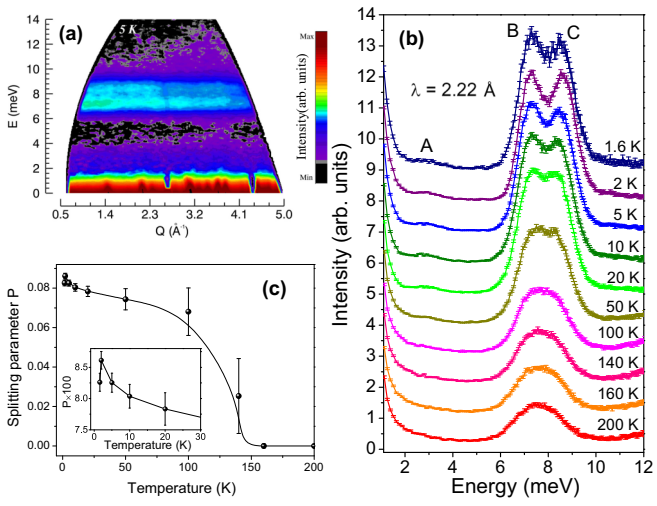

FIG. 4. (Color online) (a) The experimental Bose-factor corrected $S(Q,\omega)$ plots for NdFeAsO at 5 K obtained using an incident neutron wavelength of 2.22 Å. For clarity, a logarithmic representation is used for the intensity. (b) The temperature dependence of the CEF excitations within the energy range 2–12 meV. (c) The temperature dependence of the peak splitting parameter. The lines are guides to the eyes. The inset shows an enlarged view between 0 and 30 K.

Two peaks are clearly observed at 7.24 and 8.59 meV (labeled B and C, respectively). Their intensity decreases following the square of the magnetic form factor $F(Q)$. The evolution of the related INS spectra as a function of temperature is shown in Fig. 4(b). As the observed CEF peak intensity is proportional to the ground state transition matrix elements, $|\langle\Gamma_5^{(j)}|J_\perp|\Gamma_5^{(1)}\rangle|^2$, the marked decrease in the intensity of B and C hints at the decrease of the Van Vleck contributions to the static magnetic susceptibility. The temperature dependence of the estimated splitting parameter, $P = [E_{(C)} - E_{(B)}]/[E_{(C)} + E_{(B)}]$, reveals that the SDW transition occurs around 140 K. This is associated with a long-range antiferromagnetic order of the Fe moments. Additionally, as shown in the inset of Fig. 4(c), the splitting parameter reaches its maximum at 2 K and is reduced below 2 K. The latter finding indicates that the local potential at the Nd^{3+} sites is changed due to the change of the Fe molecular field upon the spin-reorientation transition of Fe in NdFeAsO.[13] Given the fact that the Nd moments order antiferromagnetically below 2 K in polycrystalline NdFeAsO samples,[10,12] the effective exchange field due to the Nd magnetic sublattice will influence the crystal field levels of Nd^{3+} below 2 K. A similar phenomenon has been reported for PrFeAsO,[18] in which a collapse of the splitting has been observed when the Pr sublattice orders magnetically at $T_N^{\mathrm{Pr}} = 12$ K.

The magnetic susceptibility follows the Van Vleck formula and it can be expressed in the form of matrix elements of CEF Hamiltonian. Therefore, the magnetic susceptibilities with magnetic fields applied in the *ab* plane and along the *c* axis can be calculated using the obtained CEF model Hamiltonian. The powder-averaged magnetic susceptibility can be deduced as the sum of the two magnetic field-dependent contributions, as shown in Fig. 5(a). The solid lines represent the calculated magnetic susceptibility, while the measured temperature dependence of the inverse magnetic susceptibility of the NdFeAsO powder sample are shown as open squares. The calculated susceptibility, using the CEF model, is found to be in a good agreement with the experimental data, except for the low-temperature range, in which the contribution from Fe spin density wave is present. The agreement between the measured and calculated magnetic susceptibility suggests that the obtained CEF parameters are reliable and they are able to describe the magnetic properties of NdFeAsO. Figure 5(b) shows the calculated contribution of the CEF excitations to the specific heat of NdFeAsO, employing a multilevel Schottky model. The prominent Schottky anomaly takes place at around 25 K, and the Schottky contribution extends up to high temperatures. The specific heat measurement of NdFeAsO single crystal has been performed by Tian *et al.* [Fig. 1(a) in Ref. 11]. Below 10 K, the specific heat increases with decreasing temperature. Given that the Schottky specific heat approaches zero at low temperatures due to very little probability of transition, the specific heat signal below 10 K is mainly due to the Nd magnetism and the hyperfine contribution in NdFeAsO. Above 10 K, the phonon contribution is significant and it dominates the specific heat signal. Although the calculated Schottky contribution at 25 K could not be observed clearly since it was hidden by a strong phonon signal, the calculated specific heat spreads over a reasonable range, and this is consistent with the experimental specific heat data.

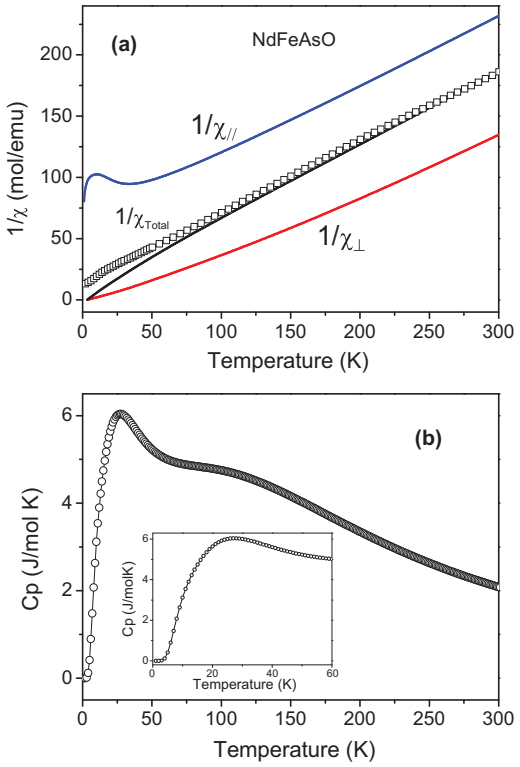

FIG. 5. (Color online) (a) Temperature dependence of the inverse magnetic susceptibility of NdFeAsO. Open squares: the experimental data. Solid lines: the calculated results according to the CEF model Hamiltonian with a field applied in the *ab* plane and along the axis, respectively. The sum curve $\chi_{\mathrm{Total}} = 1/3\chi_c + 2/3\chi_{ab}$, corresponding to the magnetic susceptibility measurement of the polycrystalline sample. (b) The calculated Schottky contribution to the specific heat for NdFeAsO. An enlarged view at the low-temperature range is shown in the inset.

IV. CONCLUSIONS

In summary, we have performed temperature-dependent inelastic neutron scattering measurements of the crystal field excitations in NdFeAsO. With decreasing tempeature, the crystal field ground state of Nd^{3+} changes from a magnetic doublet to a magnetic singlet state, accompanied by the occurrence of a long-range magnetic ordering of the Fe moments. The crystal field parameters of the Nd^{3+} ions have been determined, for both the high-temperature paramagnetic and the low-temperature antiferromagnetic phases, based on the analysis of the inelastic neutron spectra using a single-ion crystal field model Hamiltonian. The significant variation of the high-order CEF parameters, found to occur upon the magnetic phase transition, reflects a pronounced difference in the exchange interaction between the rare-earth 4*f* and conduction electrons.

ACKNOWLEDGMENT

The authors are grateful to S. Rols for providing assistance with the INS measurements.

*y.xiao@fz-juelich.de
†zbiri@ill.fr
‡chatterji@ill.fr

[1]Y. Kamihara, T. Watanabe, M. Hirano, and H. Hosono, J. Am. Chem. Soc. **130**, 3296 (2008).
[2]David C. Johnston, Adv. Phys. **59**, 803 (2010), and references therein.
[3]Z.-A. Ren, J. Yang, W. Lu, W. Yi, G.-C. Che, X.-L. Dong, L.-L. Sun, and Z.-X. Zhao, Mater. Res. Innovations **12**, 105 (2008).
[4]X. H. Chen, T. Wu, G. Wu, R. H. Liu, H. Chen, and D. F. Fang, Nature (London) **453**, 761 (2008).
[5]Z.-A. Ren, J. Yang, W. Lu, W. Yi, X.-L. Shen, Z.-C. Li, G.-C. Che, X.-L. Dong, L.-L. Sun, and F. Zhou, Europhys. Lett. **82**, 57002 (2008).
[6]H. Kito, H. Eisaki, and A. Iyo, J. Phys. Soc. Jpn. **77**, 063707 (2008).
[7]C.-H. Lee, A. Iyo, H. Eisaki, H. Kito, M. T. Fernandez-Diaz, T. Ito, K. Kihou, H. Matsuhata, M. Braden, and K. Yamada, J. Phys. Soc. Jpn. **77**, 083704 (2008).
[8]H. Maeter, H. Luetkens, Y. G. Pashkevich, A. Kwadrin, R. Khasanov, A. Amato, A. A. Gusev, K. V. Lamonova, D. A. Chervinskii, R. Klingeler, C. Hess, G. Behr, B. Büchner, and H.-H. Klauss, Phys. Rev. B **80**, 094524 (2009).
[9]S. Nandi, Y. Su, Y. Xiao, S. Price, X. F. Wang, X. H. Chen, J. Herrero-Martin, C. Mazzoli, H. C. Walker, L. Paolasini *et al.*, Phys. Rev. B **84**, 054419 (2011).
[10]Y. Qiu, Wei Bao, Q. Huang, T. Yildirim, J. M. Simmons, M. A. Green, J. W. Lynn, Y. C. Gasparovic, J. Li, T. Wu, G. Wu, and X. H. Chen, Phys. Rev. Lett. **101**, 257002 (2008).
[11]W. Tian, W. Ratcliff II, M. G. Kim, J.-Q. Yan, P. A. Kienzle, Q. Huang, B. Jensen, K. W. Dennis, R. W. McCallum, T. A. Lograsso, R. J. McQueeney, A. I. Goldman, J. W. Lynn, and A. Kreyssig, Phys. Rev. B **82**, 060514(R) (2010).
[12]T. Chatterji, G. N. Iles, B. Frick, A. Marcinkova, and J.-W. G. Bos, Phys. Rev. B **84**, 132413 (2011).
[13]A. Marcinkova, T. C. Hansen, and J.-W. G. Bos, J. Phys.: Condens. Matter **24**, 256007 (2012).
[14]P. Fulde and M. Loewenhaupt, Adv. Phys. **34**, 589 (1985).
[15]J. Jensen and A. R. Mackintosh, *Rare Earth Magnetism* (Clarendon, Oxford, 1991).
[16]A. Marcinkova, E. Suard, A. N. Fitch, S. Margadonna, and J.-W. G. Bos, Chem. Mater. **21**, 2967 (2009).
[17]S. Chi, D. T. Adroja, T. Guidi, R. Bewley, S. Li, Jun Zhao, J. W. Lynn, C. M. Brown, Y. Qiu, G. F. Chen, J. L. Lou, N. L. Wang, and P. Dai, Phys. Rev. Lett. **101**, 217002 (2008).
[18]E. A. Goremychkin, R. Osborn, C. H. Wang, M. D. Lumsden, M. A. McGuire, A. S. Sefat, B. C. Sales, D. Mandrus, H. M. Rønnow, Y. Su, and A. D. Christianson, Phys. Rev. B **83**, 212505 (2011).
[19]A generalized density of states (GDOS) is the phonon spectrum measured from inelastic neutron scattering. In contrast to the vibrational density of states (Ref. 36), the GDOS involves a weighting of the scatterers (ions) with their scattering powers σ/M (σ: cross section, M: mass).
[20]M. Zbiri, R. Mittal, S. Rols, Y. Su, Y. Xiao, H. Schober, S. L. Chaplot, M. Johnson, T. Chatterji, Y. Inoue, S. Matsuishi, H. Hosono, and Th. Brueckel, J. Phys.: Condens. Matter **22**, 315701 (2010).
[21]M. Zbiri, H. Schober, M. R. Johnson, S. Rols, R. Mittal, Y. Su, M. Rotter, and D. Johrendt, Phys. Rev. B **79**, 064511 (2009).
[22]R. Mittal, M. Zbiri, S. Rols, Y. Su, Y. Xiao, H. Schober, S. L. Chaplot, M. Johnson, T. Chatterji, S. Matsuishi, H. Hosono, and Th. Brueckel, Phys. Rev. B **79**, 214514 (2009).
[23]R. Mittal, S. Rols, M. Zbiri, Y. Su, H. Schober, S. L. Chaplot, M. Johnson, M. Tegel, T. Chatterji, S. Matsuishi, H. Hosono, D. Johrendt, and Th. Brueckel, Phys. Rev. B **79**, 144516 (2009).
[24]M. Le Tacon, M. Krisch, A. Bosak, J.-W. G. Bos, and S. Margadonna, Phys. Rev. B **78**, 140505(R) (2008).
[25]A. D. Christianson, M. D. Lumsden, O. Delaire, M. B. Stone, D. L. Abernathy, M. A. McGuire, A. S. Sefat, R. Jin, B. C. Sales, D. Mandrus, E. D. Mun, P. C. Canfield, J. Y. Y. Lin, M. Lucas, M. Kresch, J. B. Keith, B. Fultz, E. A. Goremychkin, and R. J. McQueeney, Phys. Rev. Lett. **101**, 157004 (2008).
[26]R. J. McQueeney, J. Ma, S. Chang, J.-Q. Yan, M. Hehlen, and F. Trouw, Phys. Rev. Lett. **98**, 126402 (2007).
[27]B. G. Wybourne, *Spectroscopic Properties of Rare Earths* (Interscience, New York, 1965).
[28]The CEF parameters are derived using the SAFICF program package and the MCPHASE program package.
[29]M. T. Hutchings, in *Solid State Physics*, edited by F. Seitz and D. Thurnbull (Academic, New York, 1964), Vol. 16, p. 227.
[30]P. M. Levy, J. Phys. Colloques **40**, C5-8 (1979).
[31]D. Schmitt, J. Phys. F: Metal Phys. **9**, 1745 (1979).
[32]D. Schmitt, J. Phys. F: Metal Phys. **9**, 1759 (1979).
[33]H. C. Chow, Phy. Rev. B **7**, 3404 (1973).
[34]M. Rotter and A. T. Boothroyd, Phys. Rev. B **79**, 140405(R) 2009; MCPHASE program, http://www.McPhase.de.
[35]S. Li, D. Yao, Y. Qiu, H. J. Kang, E. W. Carlson, J. Hu, G. Chen, N. Wang, and P. Dai, Front. Phys. China **5**, 161 (2010).
[36]S. N. Taraskin and S. R. Elliott, Phys. Rev. B **55**, 117 (1997).